JMEPEG (2021) 30:1603–1610
https://doi.org/10.1007/s11665-020-05253-3

1059-9495/$19.00

Physical Properties of Directionally Solidified Al-1.9Mn-5Fe Alloy

İ. Yılmazer, E. Çadırlı, H. Kaya, and U. Büyük

Submitted: 17 May 2020 / Revised: 31 August 2020 / Accepted: 3 October 2020 / Published online: 2 November 2020

Al-1.9Mn-5Fe (wt.%) alloy was prepared by adding 5 wt.% Fe to the eutectic Al-Mn alloy. This alloy undergone controlled solidification under four different growth velocities (V) in Bridgman-type furnace. Eutectic spacings (λ), microhardness (HV), ultimate tensile strength (σ_U) and electrical resistivity (ρ) of these alloys were determined. While the HV and σ_U increased with increasing V values or decreasing λ, the elongation (δ) values decreased. In addition, relationships between these parameters were investigated using linear regression analysis. Microstructure photographs of directionally solidified samples were taken by optical microscope and scanning electron microscope (SEM). The eutectic spacings were measured from these photographs. The relationships among growth velocity (V), eutectic spacing (λ), microhardness (HV), ultimate tensile strength (σ_U) and electrical resistivity (ρ) were measured by suitable method and tests. The ρ measurements were carried out depending on V and temperature (T). While temperature coefficient of resistivity (α_{TCR}) was calculated from the ρ–T curve, the values of thermal conductivity (K) predicted by Wiedemann–Franz (W–F) and Smith–Palmer (S–P) equations. It was found that the microstructure, microhardness, tensile strength and electrical resistivity were affected by both eutectic spacing and the growth velocity.

Keywords eutectic spacing, microhardness, resistivity, tensile strength, thermal conductivity

1. Introduction

The alloying components added to the aluminum further improve the properties of the material, making it superior to other metals. Aluminum and aluminum alloys are the most important metal group after iron-based materials in the world. It is also the most used among light metals both in pure form and in alloys (Ref 1-10). Aluminum alloys composed with the addition of copper, silicon, iron, zinc, magnesium, manganese, nickel, titanium and many others to the aluminum. One or a combination of those cited elements can be used to form these alloys. Alloying elements added to aluminum can be classified with their supplemental properties as castability, mechanical strength, chemical stability, workability, thermal expansion, thermal conductivity and heat resistance (Ref 1). The physical properties of the Al-Mn alloy formed with alloying elements as Cu, Si, Fe by solidifying it in a controlled directionally form in either fast or cast form by Bridgman-type furnace have been reported in the literature, but the results differ from each other (Ref 11-16).

In equilibrium conditions at 927.14 K, the maximum solubility of Fe in Al is 0.046 wt.% Fe. In Fe-containing alloys, the maximum solubility of Mn may be approximately half that of binary Al-Mn alloys (Ref 17). Binary alloys have a limited application area, because commercial Al alloys always contain appreciable amounts of Fe, which significantly affects the microstructure. Intermetallic compounds (IMCs) formed during solidification due to the more tendency of the Fe atoms to segregate contain relatively more Fe than Mn. This is called inverse segregation of Fe due to the gravity (Ref 18-20). Information on IMC phase structures formed in Al-rich Al-Mn-Fe ternary alloy has been reported in detail in some previous studies (Ref 7-9). The IMC phases according to the Fe:Mn ratios are defined as Al_3 (Fe, Mn) or Al_6 (Mn, Fe). The microstructures containing IMC phase/phases play a significant role on the physical properties of the material (Ref 8). Therefore, the Al-Mn-Fe alloy is an important commercial aluminum alloy. It has been used in many industrial sectors (such as packaging (Al foil), architectural plate, lithography plate, air-conditioning and insulation), especially in the rapidly growing aluminum heat exchanger sector (Ref 21, 22). In this study, the physical properties have been investigated depending on growth velocities in the Al-1.9Mn-5Fe (wt.%) ternary eutectic alloy, which has commercial and industrial importance (Ref 23-25). Since the growth velocity affects the microstructure significantly, it is an inevitable fact that the mechanical, thermal and electrical properties of the studied alloy are affected by the solidification conditions. Indeed, thermophysical properties like molar heat capacity, thermal conductivity, electrical conductivity, latent heat, transformation heat, all depend on the nucleation rate (Ref 26). Directional solidification of the Al-1.9Mn-5Fe ternary alloy under certain conditions is an important issue in obtaining the fine-grained microstructure required for the desired favorable material properties. Still very limited work has reported systematically about the influences of the growth velocity and cooling rate on the modification of Al-Mn and Al-Mn-Fe alloys. The aim of present study was experimentally investigate the effect of growth velocity (V) on the microstructure, mechanical and

İ. Yılmazer, H. Kaya, and **U. Büyük**, Department of Science Education, Faculty of Education, Erciyes University, Kayseri, Turkey; and **E. Çadırlı**, Department of Physics, Faculty of Arts and Sciences, Niğde Ömer Halisdemir University, Niğde, Turkey. Contact e-mail: ecadirli@gmail.com.

electrical properties of Al-1.9Mn-5Fe ternary alloy. And also, another aim is to determination of the relationships among V, λ, HV, σ_U and ρ.

2. Experimental Procedures

2.1 Alloy Preparation, Solidification and Metallographic Processes

Al-1.9Mn-5Fe alloy was produced under a vacuum atmosphere by using 99.99% purity Al, Mn and Fe metals taking into account the phase diagram (Ref 27). All chemical compositions are given in weight percent (wt.%) throughout this paper. Solidification of the samples was carried out with different V (from 8.3 to 978 μm/s) at a constant G (6.7 K/mm), in a Bridgman-type furnace. After about 10 cm of solidification, the samples were quenched by rapidly pulling it down into the water reservoir. After quenching the samples, they were subjected to standard metallography process such as cutting, grinding, polishing (with 3, 1 and 0.25 μm diamond pasts) and etching (10 mL sulfuric, 5 mL hydrofluoric acid and 85 mL H_2O for 15 s at room temperature). More details of the experimental procedures are given in (Ref 2, 5).

2.2 Measurements of Eutectic Spacing (λ), Microhardness (HV) and Tensile Strength (σ)

Different methods have been used to measure of eutectic spacings (λ_L, λ_T) on the microstructure. Measurements of the eutectic spacings were made from both the longitudinal (λ_L) and transverse section (λ_T) of the samples by using linear intersection method. The details of the eutectic spacing measurements are given based on the features described in the previous study (Ref 28). The microhardness measurements were performed a digital microhardness test apparatus. In the microhardness measurements, approximately twenty measurements were made from different regions on both the longitudinal section and the transverse section of the directionally solidified sample at each V value and their average values were used for statistical reliability. Tensile strength tests were made with a fully automatic testing apparatus adjustable to different strain rates. In these tests, cylindrical samples with a length of 60 mm and a diameter of 4 mm were prepared and subjected to tensile testing at a strain rate of 10^{-3} s^{-1}. For statistical reliability, this test was repeated three times for each V value and the average value was used (more details are provided in Ref 29).

2.3 Measurements of Electrical Resistivity (ρ)

In this study, the "Four Point Probe Method" was used to measure the ρ of studied alloy. To determine the dependence of ρ on V at room temperature (R.T.), ρ measurements were made on the longitudinal section of the solidified samples with different V. Also, ρ measurements were carried out depending on the temperature.

2.4 Prediction of Thermal Conductivity (K)

The relationship between the K and σ has been suggested by Wiedemann–Franz (W–F) (Ref 30). Later, the modification of the W–F equation was developed by Smith–Palmer (S–P) (Ref 31). The variations of K with T were predicted from the W–F ($K = \sigma LT$) and S–P ($K = 0.909\ \sigma LT + 10.5$) equations by using the measured values of electrical resistivity ($\rho = 1/\sigma$). L is the Lorenz constant and its value is 2.45×10^{-8} W Ω/K^2. The details of ρ measurements and predicted K values were described in (Ref 32).

3. Results and Discussion

3.1 Composition Analysis of the Phases

EDX analysis was performed to determine the composition of the phases in the Al-1.9Mn-5Fe alloy at 20 keV using the x-ray lines (LEO 440 model). According to EDX spectrums as shown in Fig. 1 and the quantity of components in each phases, black rod eutectic phase (white rectangular frame), quenched liquid phase (yellow rectangular frame), gray phase (blue rectangular frame) and white plate phase (dark rectangular frame) were identified as Al_6Fe intermetallic phase (rod-like eutectic), Al-rich α-Al phase, solid Al phase and Al_6FeMn intermetallic phase (plate-like eutectic), respectively. The composition of α-Al phase (Al-1Mn-4.6Fe) is close to nominal composition (Al-1.9Mn-5Fe). The main phase and intermetallic phases were confirmed by XRD analysis in the previous work of Çadırlı et al.(Ref 29).

3.2 The Effect of V on λ

Figure 2 shows the eutectic microstructures of the studied alloy. The eutectic spacings were measured from both the longitudinal and transverse sections of samples. As seen from Fig. 2, microstructure is usually rod eutectic (Al_6Fe IMC's) form on longitudinal sections of the samples (Fig. 2a, c, e). However, plate-like eutectic (Al_6FeMn IMC's) fibers (Fig. 2b, d, f) were frequently observed in the microstructure (transverse section) of the studied alloy. With increasing the growth velocity (8.3-978 μm/s) at a constant G (6.7 K/mm), grain size of eutectic fibers (Al_6FeMn and Al_6Fe IMC's) and the spacings between them reduced and microstructure highly refined (Fig. 2e, f). As seen in Fig. 3, when the V was increased from 8.3 to 978 μm/s, the λ_L value decreased from 12.7 to 2.5 μm and the λ_T value decreased from 11.9 to 1.5 μm. The relationships between λ_L, λ_T and V were obtained by binary regression analysis and are given in Table 1. The exponent values of the V for λ_L and λ_T are 0.34 and 0.43, respectively. The exponent value of the V (0.43) for λ_T is in good agreement with values reported by different researchers (Ref 33-37).

3.3 The Effects of V and λ on HV

An increase in the V (or decrease of the λ) resulted in increased HV (Fig. 4, 5). When the V was increased from 8.3 to 978 μm/s, the HV_L increased from 34.7 to 44.7 kg/mm^2 and the HV_T increased from 37.2 to 51.9 kg/mm^2. The values of the exponential of V for HV_L and HV_T are found to be as 0.05 and 0.07, respectively. These values are compatible with some values available in the literature (Ref 38-40), but differ with some values (Ref 41-44). These differences are due to factors such as alloy composition, impurities in the sample, solidification conditions and calibration settings of the test device.

3.4 The Effects of V and λ on σ_U

Stress–strain curves for different V values and $\sigma_U - V$ plot were given in the previous study of Çadırlı et al. (Ref 29).

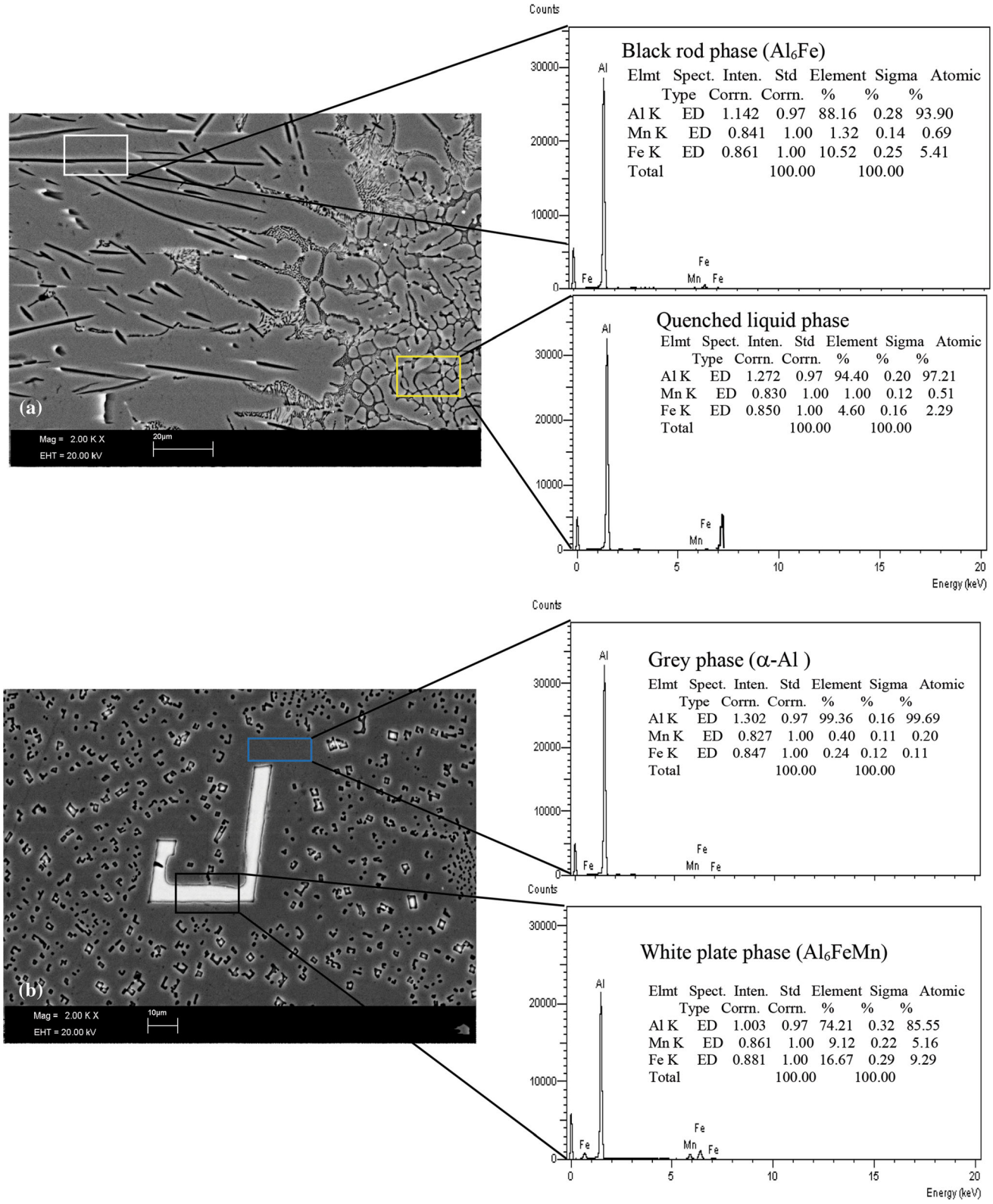

Fig. 1 Chemical composition analysis of Al-1.9Mn-5Fe alloy with the EDX (a) longitudinal section, (b) transverse section

While increasing σ_U with increasing V, elongation values (δ) tended to decrease. While the V increases from 8.3 to 978 μm/s, the values of σ_U increased from 153.9 to 192.3 MPa, but δ values decreased from 0.90 to 0.39% (Table 2). The increase in HV according to increasing V is slightly larger compared to the increase in σ_U, which could be due to the presence of IMC phases (Al_6FeMn and Al_6Fe) present at the grain boundaries. By consequence, the increase in HV of the phase is more noticeable than the increase in the strength of the whole alloy. The refinement of the eutectic microstructure is remarkable

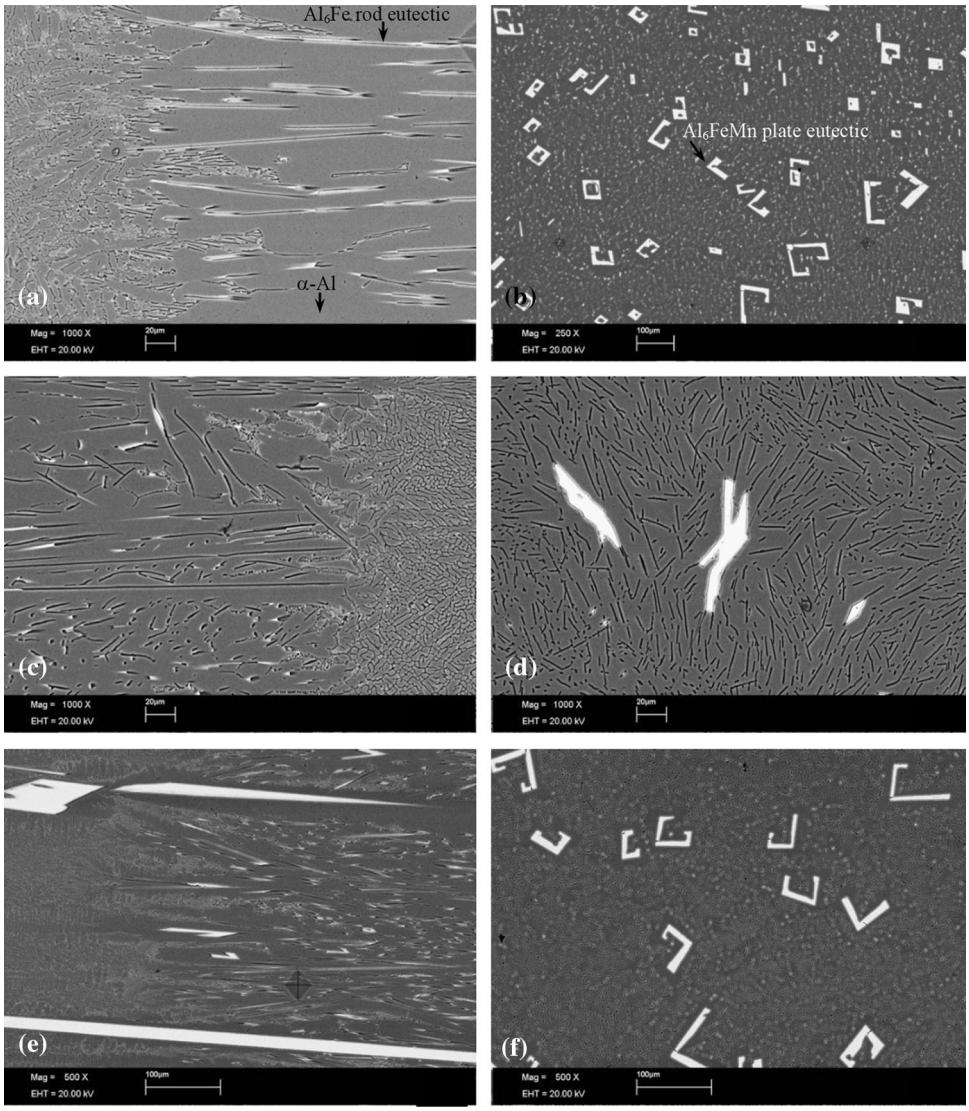

Fig. 2 SEM photographs of microstructures formed under different growth velocities (V = 8.3-978 μm/s) at constant temperature gradient (G = 6.7 K/mm) for directionally solidified Al-1.9Mn-5Fe alloy (a) longitudinal section (b) transverse section (V = 8.3 μm/s, G = 6.7 K/mm), (c) longitudinal section (d) transverse section (V = 41.6 μm/s, G = 6.7 K/mm), (e) longitudinal section (f) transverse section (V = 978 μm/s, G = 6.7 K/mm)

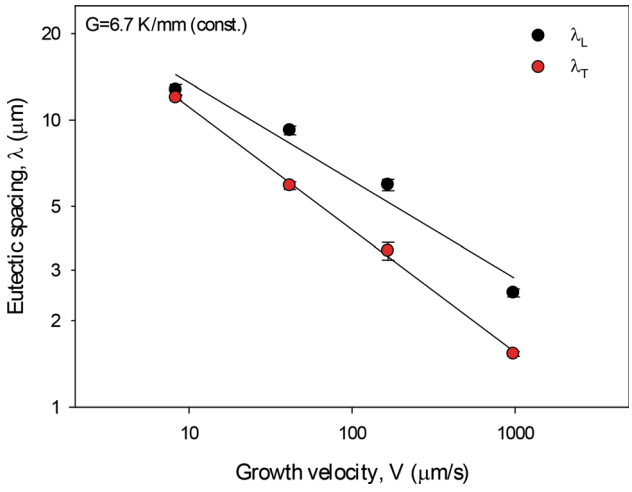

Fig. 3 Variation of the eutectic spacing with growth velocity

locally in the phase, but the effect on the degree of reinforcement the alloy depends on its volume fraction and other phase properties (Ref 20). As can be seen from Table 1, the exponent value of V for σ_U is equal to 0.05. This exponent value (0.05) is close to the values reported by some researchers (Ref 38, 40). Figure 6 shows that the σ_U values change according to the λ values. While the value of λ decreases from 11.9 to 1.5 μm, the value of σ_U increases from 153.8 to 192.3 MPa. A similar trend has been reported by Shaha et al. (Ref 45). As shown in Table 1, the exponent value of λ is obtained as 0.11. This exponent value is fairly close to value of 0.12 obtained by Shabestari and Shahri (Ref 46).

The identity, shape, size and distribution of the IMC phases are critical influences on the material properties of the alloy including HV and σ_U [25]. In the present study, the size of the Al_6Fe and Al_6FeMn eutectic fibers and the spacings between them decreased substantially with increasing V. Smaller eutectic spacings can be associated with a more homogeneous distribution of Al_6Fe eutectic fibers in the Al-rich matrix phase,

Table 1 The experimental relationships among λ, HV, σ_U and ρ obtained by binary regression analysis

Relationships	Experimental constants, k	Correlation coefficients, r
$\lambda_T = k_1 V^{-0.43}$	$k_1 = 29.7$, $\mu m^{1.43}$ $s^{-0.43}$	$r_1 = -0.998$
$\lambda_L = k_2 V^{-0.34}$	$k_2 = 29.6$, $\mu m^{1.34}$ $s^{-0.34}$	$r_2 = -0.979$
$HV_T = k_3 V^{0.07}$	$k_3 = 50.0$, kg $mm^{-2.07}$ $s^{0.07}$	$r_3 = 0.963$
$HV_L = k_4 V^{0.05}$	$k_4 = 42.9$, kg $mm^{-2.05}$ $s^{0.05}$	$r_4 = 0.976$
$HV_T = k_5 \lambda_T^{-0.17}$	$k_5 = 17.3$, kg $mm^{-1.83}$	$r_5 = -0.966$
$HV_L = k_6 \lambda_L^{-0.16}$	$k_6 = 17.5$, kg $mm^{-1.84}$	$r_6 = -0.999$
$\sigma_U = k_7 V^{0.05}$	$k_7 = 138.8$, MPa $mm^{-0.05}$ $s^{0.05}$	$r_7 = 0.992$
$\sigma_U = k_8 \lambda^{-0.11}$	$k_8 = 203.2$, MPa $\mu m^{0.11}$	$r_8 = -0.987$
$\rho = k_9 V^{0.12}$	$k_9 = 2 \times 10^{-7}$, Ω $m^{0.88}$ $s^{0.12}$	$r_9 = 0.997$

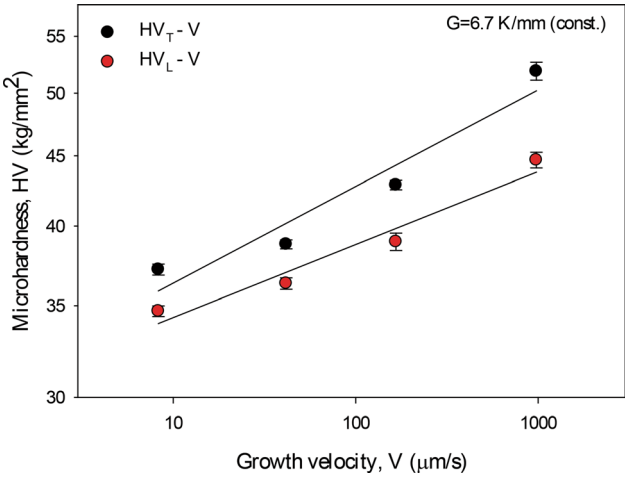

Fig. 4 Variation of the microhardness with growth velocity

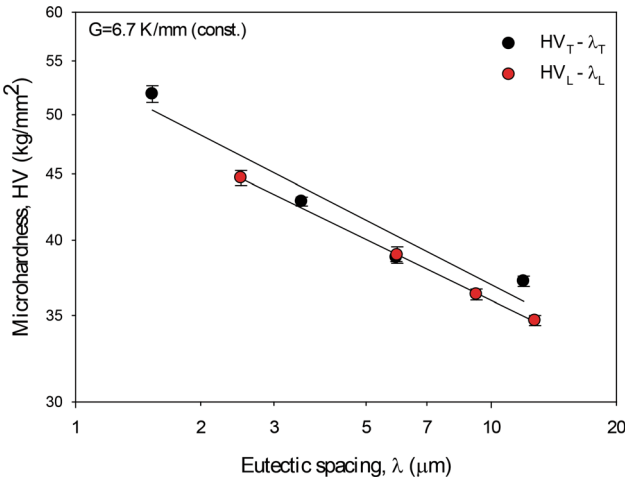

Fig. 5 Variation of the microhardness with eutectic spacing

thus contributing to the increase in the HV and σ_U, as they will effectively contribute to block the dislocation movement initiated in the ductile α-Al matrix phase.

3.5 Effects of V and T on the ρ

Variation of ρ as a function of V at R.T is given in Fig. 7. The ρ value increased from 5×10^{-8} to 9×10^{-8} Ω m with the increase in V from 8.3 to 978 μm/s. Thus, the ρ value

Table 2 σ_U and δ values according to growth velocity (Ref 29)

V, μm/s	σ_U, MPa	δ, %
8.3	153.9	0.90
41.6	164.7	0.81
166.3	180.7	0.68
978.0	192.3	0.39

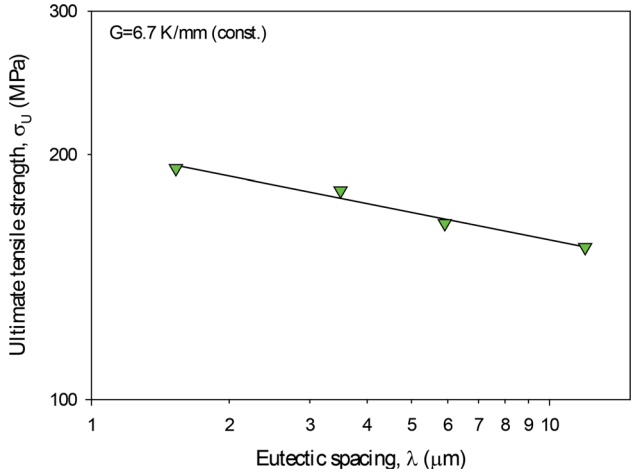

Fig. 6 Variation of the ultimate tensile strength with eutectic spacing

increased up to 80%. The V has been quite effective on the ρ. Relationship between V and ρ is determined by linear regression analysis. This empirical relationship is given in Table 1. The exponent value of V for ρ is obtained as 0.12. This exponent value is the same as the exponent value (0.12) reported by Engin et al. (Ref 39) for Al-6.5Ni-1.5Fe alloy.

Variation of ρ depending on T for the studied alloy in the range of 287-584 K is seen in Fig. 8. The ρ increases nearly linearly with increasing T. Namely, with increasing T from 287 to 584 K, the values of ρ increase 5×10^{-8} to 17.6×10^{-8} Ω m. The temperature coefficient of resistivity ($\alpha_{TCR} = 4.66 \times 10^{-3}$ K^{-1}) was determined from the $\rho - T$ curve in the temperature range of 287-584 K. The increment of ρ should be mainly attributed to the increasing of intermetallic and vacancies in the Al matrix. The ρ–T curve constitutes a typical behavior of metallic alloys. The IMC phases, impurities

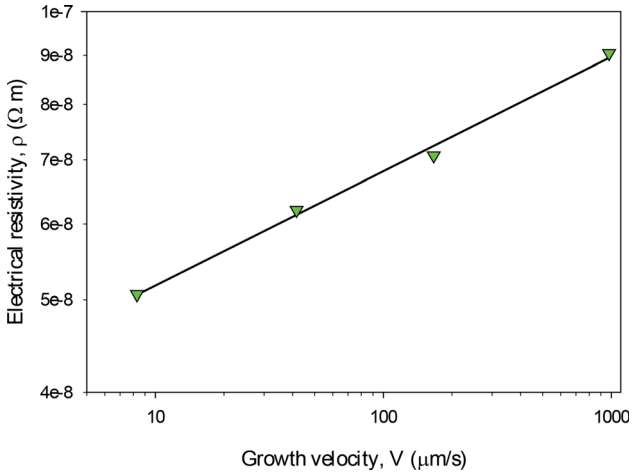

Fig. 7 Variation of the electrical resistivity with growth velocity at room temperature

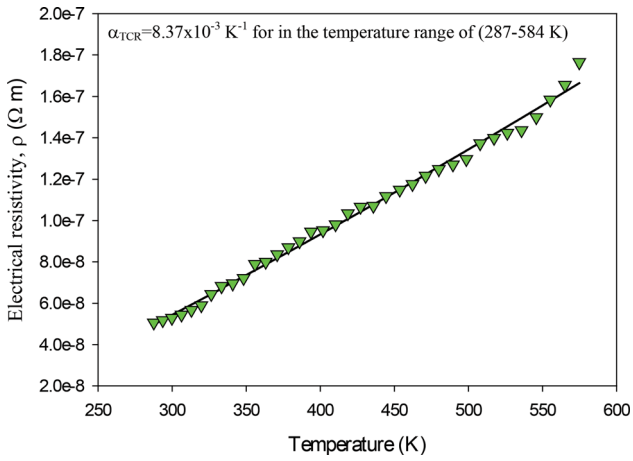

Fig. 8 The electrical resistivity versus temperature curve of the solidified sample under certain conditions (G = 6.7 K/mm and V = 8.3 μm/s)

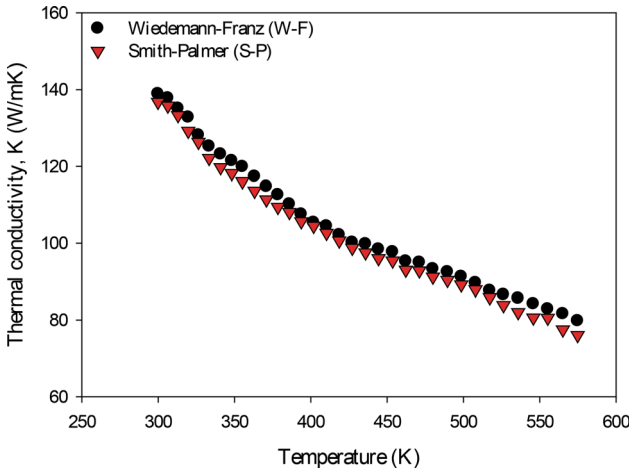

Fig. 9 Variation of K values predicted from the Wiedemann–Franz and Smith–Palmer equations with temperature

and vacancy defects are present within the matrix phase (α-Al). It is known that changes in the resistivity of the metals are depended by the changes to the mean time between the conduction electrons collisions which will depend on the IMC formed in matrix phase. Increased resistivity is inevitable due to the more scattering of electrons with current carriers in metals and metallic alloys, and the decrease in their mean free paths. Thus, resistivity is sensitive to initial nucleation of the IMC phases, their growth and coarsening and finally their dissolution in the matrix. The effect of impurity atoms and IMC phases played a major role in the formation of such behavior (Ref 47). Therefore, it is reasonable to conclude that mutual interaction of intermetallic phases and dislocation movement is responsible for ρ in the studied alloy.

3.6 Prediction of K

K values predicted from W–F (Ref 30) and S–P (Ref 31) equations by using experimental measured ρ values for each temperature are given in Fig. 9. K values in this plot are found to be in the ranges of 79-139 W/mK and 76-137 W/mK for W–F and S–P equations, respectively. The K values estimated from W–F equation are slightly higher than the K values estimated from S to P equation. A temperature increases from R.T to 577 K resulted in a decrease in the values of K up to 45%. The effect of T on ρ is much greater than K.

4. Conclusions

In this work, the eutectic spacings (λ_L, λ_T), the mechanical properties (HV_L, HV_T, σ_U and δ), ρ and K of the studied alloy were investigated. The relationships between these physical properties with V and λ have been determined.

1. The λ values are getting smaller according to the increasing V values, and the microstructure has evolved into a finer grain structure. Therefore, the homogeneous distribution of eutectic spacings tends to improve the mechanical properties of the studied alloy.
2. The λ_L and λ_T decreased with increasing V. The relationships between the λ_L, λ_T and V were obtained as (λ_T = 29.7 $V^{-0.43}$, λ_L = 29.6 $V^{-0.34}$).
3. The values of HV increased significantly according to increasing V and decreasing λ values. The experimental relationships between these parameters are given as (HV_T = 50 $V^{0.07}$, HV_L = 42.9 $V^{0.05}$, HV_T = 17.3 $\lambda_T^{-0.17}$, HV_L = 17.5 $\lambda_L^{-0.16}$).
4. The values of σ_U increased with increasing V and decreasing λ. Besides, elongation (δ) values decreased significantly. The experimental relationships between these parameters are given as (σ_U = 138.8 $V^{0.05}$, σ_U = 203.2 $\lambda^{-0.11}$).
5. The relationship between ρ and V was found to be $\rho = 2 \times 10^{-7}$ $V^{0.12}$. Also, ρ values nearly linear increased with increasing T and α_{TCR} was determined as 8.37×10^{-3} K^{-1}.
6. The K variations with T were predicted from W–F and S–P equations by using experimentally measured ρ values in related equations. According to these predictions, K values decreased from 139 to 79 W/mK with increasing T.

Acknowledgments

This work was supported by the ERU, Scientific Research Project Unit (FBA-2015-5631). The authors are grateful for the supports to ERU Scientific Research Project Unit.

References

1. E.J. Lavernia and N.J. Grant, Aluminium-Lithium Alloys, *J. Mater. Sci.*, 1987, **22**, p 1521–1529
2. M. Gündüz and E. Çadırlı, Directional Solidification of Aluminium–Copper Alloys, *Mater. Sci. Eng. A*, 2002, **327**, p 167–185
3. H. Kaya, U. Böyük, E. Çadırlı, and N. Maraşlı, Influence of Growth Rate on Microstructure, Microhardness and Electrical Resistivity of Directionally Solidified Al-7 wt.% Ni Hypo-Eutectic Alloy, *Met. Mater. Int.*, 2013, **19**, p 39–44
4. E. Çadırlı, Effect of Cooling Rate and Composition on Mechanical Properties of the Directionally Solidified Al-rich Al-Cu Alloys, *Met. Mater. Int.*, 2013, **19**, p 411–422
5. E. Çadırlı, E. Nergiz, H. Kaya, U. Büyük, M. Şahin, and M. Gündüz, Effect of Growth Velocity on Microstructure and Mechanical Properties of Directionally Solidified 7075 Alloy, *Int. J. Cast Met. Res.*, 2020, **33**, p 11–23
6. Q. Zhao, Z. Qian, X. Cui, Y. Wu, and X. Liu, Optimizing Microstructures of Dilute Al-Fe-Si Alloys Designed with Enhanced Electrical Conductivity and Tensile Strength, *J. Alloys Compd.*, 2015, **650**, p 768–776
7. D. Pavlyuchkov, S. Balanetskyy, W. Kowalski, M. Surowiec, and B. Grushko, Stable Decagonal Quasicrystals in the Al-Fe-Cr and Al-Fe-Mn Alloy Systems, *J. Alloys Compd.*, 2009, **477**, p L41–L44
8. O. Engler, G. Laptyeva, and N. Wang, Impact of Homogenization on Microchemistry and Recrystallization of the Al-Fe-Mn Alloy AA 8006, *Mater. Charact.*, 2013, **79**, p 60–75
9. S. Balanetskyy, D. Pavlyuchkov, T. Velikanova, and B. Grushko, The Al-Rich Region of the Al-Fe-Mn alloy system, *J. Alloys Compd.*, 2015, **619**, p 211–220
10. R. Oliveira, R. Kakitani, L.R. Ramos, D.L. Gonçalves, A. Garcia, and N. Cheung, The Roles of Mn and Ni Additions to Fe Contaminated Al in Neutralizing Fe and Stabilizing the Cellular α-Al Microstructure, *J. Sustain. Metall.*, 2019, **5**, p 561–580
11. W.W. Zhang, B. Lin, D.T. Zhang, and Y.Y. Li, Microstructures and Mechanical Properties of Squeeze Cast Al-5.0Cu-0.6Mn Alloys with Different Fe Content, *Mater. Design.*, 2013, **52**, p 225–233
12. I.J. Polmear, *Light Alloys: Metallurgy of the Light Metals*, Wiley, Hoboken, 1995
13. W.T. Denholm, J.D. Esdaile, N.G. Siviour, and B.W. Wilson, The Nature of the $FeAl_3$ Liquid $(FeMn)Al_6$ Reaction in the Al-Fe-Mn System, *Metall. Mater. Trans. A*, 1987, **18**, p 393–397
14. S.G. Shabestari, The Effect Fe and Mn on Formation of Intermetallic Compounds in Al-Si Alloys, *Mater. Sci. Eng. A*, 2004, **383**, p 289–298
15. J.Y. Hwang, H.W. Doty, and M.J. Kaufman, The Effects of Mn Additions on the Microstructure and Mechanical Properties of Al-Si-Cu Casting Alloys, *Mater. Sci. Eng. A.*, 2008, **488**, p 496–504
16. C.M. Dinnis, J.A. Taylor, and A.K. Dahle, Interactions Between Iron, Manganese, and the Al-Si Eutectic in Hypoeutectic Al-Si Alloys, *Metall. Mater. Trans. A*, 2006, **37**, p 3283–3291
17. L.F. Mondolfo, *Manganese in Aluminum Alloys*, The Manganese Centre, Paris, 1978
18. R. Mehrabian, M. Kaene, and M.C. Flemings, Interdendritic Fluid Flow and Macrosegregation; Influence of Gravity, *Met. Trans*, 1970, **1**, p 1209–1220
19. D.G. Eskin, J. Zuidema, V.I. Savran, and L. Katgerman, Structure Formation and Macrosegregation Under Different Process Conditions During DC Casting, *Mater. Sci. Eng. A*, 2004, **384**, p 232–244
20. A.P. Boeira, I.L. Ferreira, and A. Garcia, Alloy Composition and Metal/Mold Heat Transfer Efficiency Affecting Inverse Segregation and Porosity of As-Cast Al–Cu Alloys, *Mater. Des.*, 2009, **30**, p 2090–2098
21. C.M. Allen, S. Kumar, L. Carrol, K.A.Q. O'Reilly, and H. Cama, Electron Beam Surface Melting of Model 1200 Al alloys, *Mater. Sci. Eng. A*, 2001, **304–306**, p 604–607
22. M. Karlik, J. Siegl, M. Slamova, and Y. Birol, Study of the Damage of AA 8006 Twin-Roll Cast Thin Sheets During Forming of Heat Exchanger Fins, *Mater. Sci. Forum*, 2000, **331–337**, p 619–624
23. B. Dutta and M. Rettenmayr, Effect of Cooling Rate on the Solidification Behaviour of Al-Fe-Si Alloys, *Mater. Sci. Eng. A*, 2000, **283**, p 218–224
24. Y.H. Zhang, Y.C. Liu, Y.J. Han, C. Wei, and Z.M. Gao, The Role of Cooling Rate in the Microstructure of Al-Fe-Si Alloy with High Fe and Si Contents, *J. Alloys Compd.*, 2009, **473**, p 442–445
25. P.R. Goulart, J.E. Spinelli, N. Cheung, and A. Garcia, The Effects of Cell Spacing and Distribution of Intermetallic Fibers on the Mechanical Properties of Hypoeutectic Al-Fe Alloys, *Mater. Chem. Phys.*, 2010, **119**, p 272–278
26. I.L. Ferreira, J.A. de Castro, and A. Garcia, Determination of Heat Capacity of Pure Metals, Compounds and Alloys by Analytical and Numerical Methods, *Thermochim. Acta*, 2019, **682**, p 178418
27. J.R. Davis, Ed., *ASM Specialty Handbook: Aluminum and Aluminum Alloys*, ASM International, Materials Park, 1993
28. E. Çadırlı, U. Boyuk, S. Engin, H. Kaya, N. Maraşlı, and A. Ülgen, Experimental Investigation of the Effect of Solidification Processing Parameters on the Rod Spacings in the Sn-1.2 wt.% Cu Alloy, *J. Alloys Compd.*, 2009, **486**, p 199–206
29. E. Çadırlı, A. Aker, Y. Kaygısız, and M. Şahin, Influences of Growth Velocity and Fe Content on Microstructure, Microhardness and Tensile Properties of Directionally Solidified Al-1.9Mn-xFe Ternary Alloys, *Mater. Res.*, 2017, **20**, p 801–813
30. C. Kittel, *Introduction to Solid State Physics*, 6th ed., Wiley, New York, 1965
31. D.R. Poirier and G.H. Geiger, *Transport Phenomena in Materials Processing*, Metals and Materials Society, Pittsburgh, Mineral, 1994
32. E. Çadırlı, M. Şahin, R. Kayalı, M. Arı, and S. Durmuş, Dependence of Electrical and Thermal Conductivity on Temperature in Directionally Solidified Sn-3.5 wt.% Ag Eutectic Alloy, *J. Mater. Sci. Mater. Electron.*, 2011, **22**, p 1709–1714
33. M. Gündüz, H. Kaya, E. Çadırlı, and A. Özmen, Interflake Spacings and Undercoolings in Al-Si Irregular Eutectic Alloy, *Mater. Sci. Eng. A*, 2004, **369**, p 215–229
34. S. Steinbach and L. Ratke, The Influence of Fluid Flow on the Microstructure of Directionally Solidified AlSi-Base Alloys, *Metall. Mater. Trans. A*, 2007, **38**, p 1388–1394
35. A. Aker, S. Engin, İ. Yılmazer, and H. Kaya, Influence of the Growth Rate on Physical Properties in the Aluminum-Antimony Eutectic Alloy, *Int. J. Mater. Eng. Technol.*, 2013, **9**, p 59–76
36. J. Fan, X. Li, Y. Su, J. Guo, and H. Fu, The Microstructure Parameters and Microhardness of Directionally Solidified Ti-43Al-3Si Alloy, *J. Alloys Compd.*, 2010, **506**, p 593–599
37. E. Çadırlı, İ. Yılmazer, M. Sahin, and H. Kaya, Investigation of the Some Physical Properties of the Directionally Solidified Al-Cu-Co Ternary Eutectic Alloy, *Trans. Indian Inst. Met.*, 2015, **68**, p 817–827
38. J.T. Guo, C.M. Xu, X.H. Du, and H. Fu, The Effect of Solidification Rate on Microstructure and Mechanical Properties of an Eutectic NiAl-Cr(Mo)-Hf Alloy, *Mater. Lett.*, 2004, **58**, p 3233–3236
39. S. Engin, U. Büyük, and N. Maraşlı, The Effects of Microstructure and Growth Rate on Microhardness, Tensile Strength, and Electrical Resistivity for Directionally Solidified Al-Ni-Fe Alloys, *J. Alloy. Compd.*, 2016, **660**, p 21–23
40. J. Lapin and J. Marecek, Effect of Growth Rate on Microstructure and Mechanical Properties of Directionally Solidified Multiphase Intermetallic Ni-Al-Cr-Ta-Mo-Zr Alloy, *Intermetallics*, 2006, **14**, p 1339–1344
41. J. Lapin, L. Ondrus, and M. Nazmy, Directional Solidification of Intermetallic Ti-46Al-2W-0.5Si Alloy in Alumina Moulds, *Intermetallics*, 2002, **10**, p 1019–1031
42. J. Fan, X. Li, Y. Su, J. Guo, and H. Fu, Dependency of Microhardness on Solidification Processing Parameters and Microstructure Characteristics in the Directionally Solidified Ti-46Al-0.5W-0.5Si Alloy, *J. Alloy Compd.*, 2010, **504**, p 60–64
43. S. Khan, A. Ourdjini, Q.S. Hamed, M.A.A. Najafabadi, and R. Elliott, Hardness and Mechanical Property Relationships in Directionally Solidified Aluminium-Silicon Eutectic Alloys with Different Silicon Morphologies, *J. Mater. Sci.*, 1993, **28**, p 5957–5962
44. U. Böyük, N. Maraşlı, E. Çadırlı, H. Kaya, and K. Keşlioğlu, Variations of Microhardness with Solidification Parameters and

Electrical Resistivity with Temperature for Al-Cu-Ag Eutectic Alloy, *Curr. App. Phys.*, 2012, **12**, p 7–10
45. S.K. Shaha, F. Czerwinski, W. Kasprzak, J. Friedman, and D.I. Chen, Effect of Solidification Rate and Loading Mode on Deformation Behavior of Cast Al-Si-Cu-Mg Alloy with Additions of Transition Metals, *Mater. Sci. Eng. A*, 2015, **636**, p 361–372
46. S.G. Shabestari and F. Shahri, Influence of Modification, Solidification Conditions and Heat Treatment on the Microstructure and Mechanical Properties of A356 Aluminum Alloy, *J. Mater. Sci.*, 2004, **39**, p 2023–2032
47. D.D. Pollock, *Electrical Conduction in Solids: An Introduction*, ASM, Metals Park, 1985